The Canadian Model of Ocean Carbon (CMOC) v1.0

Konstantin Zahariev[1], James R. Christian[1,2], Kenneth L. Denman[1,2]

[1] *Canadian Centre for Climate Modelling and Analysis, c/o University of Victoria, PO Box 1700 STN CSC, Victoria, British Columbia, Canada V8W 2Y2*

[2] *Fisheries and Oceans Canada, Institute of Ocean Sciences, PO Box 6000, Sidney, British Columbia, Canada V8L 4B2*

E-mail: kos.zahariev@ec.gc.ca

- - revised Jul 31, 2007

- - revised Aug 23, 2006

- - revised Jan 19, 2006

- - revised Jan 17, 2006

Contents

List of Figures

Chapter 1

Introduction

A global ocean carbon model, the Canadian Model of Ocean Carbon (CMOC), is described as a carbon cycle component in the coupled Canadian Centre for Climate Modelling and Analysis (CCCma) atmosphere-ocean general circulation model (GCM).

It consists of CCCma's ocean general circulation model with an embedded inorganic chemistry module, a four-plus-one-component NPZD ecosystem model with dynamic chlorophyll, and a parameterized carbonate pump (Figure 1.1). Phytoplankton growth in the model is limited by light, temperature, nutrients, and iron. Iron limitation is applied as a geographical mask based on annual minimum observed nitrate concentration. Variable Chl:N ratio has been implemented to account for phytoplankton photoacclimation to light availability, with chlorophyll as a separate prognostic quantity. The model includes parameterizations of photoacclimation, dinitrogen fixation, and calcification/calcite dissolution.

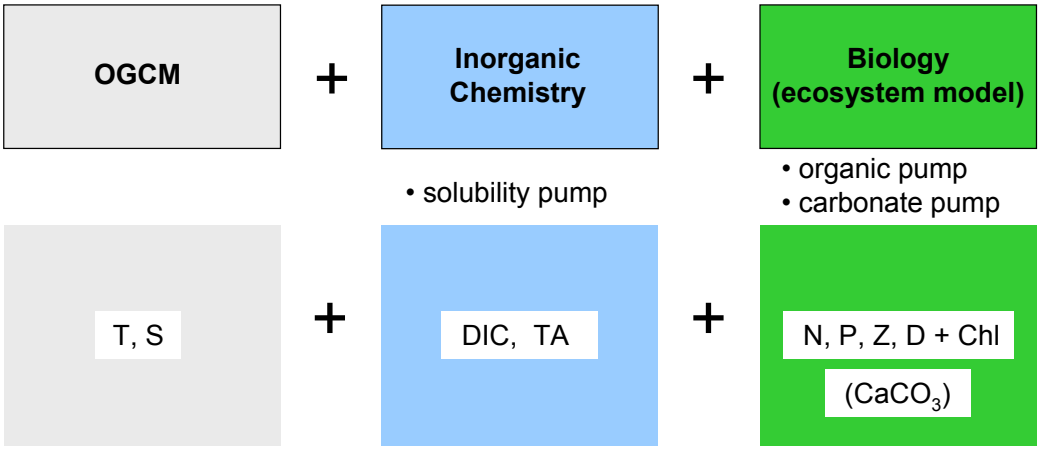

FIG. 1.1. CMOC v.1.0: Summary

1.1 OVERVIEW

We have coupled a modified version of an NPZD ecosystem model, similar to the 1-D model by Denman and Peña (1999), to a global carbon ocean model. The five ecosystem variables are Nitrogen, Phytoplankton, Zooplankton and Detritus, and Chlorophyll. The inorganic chemistry module variables are dissolved inorganic carbon (DIC) and total alkalinity (TA) for a total of seven prognostic variables related to the ocean carbon cycle.

Phytoplankton growth is limited by light, temperature, nitrogen, and iron. Detritus sinks with a constant speed, and export production is calculated at the bottom of the euphotic zone. $CaCO_3$ formation is represented implicitly as a temperature-varying fraction of the export production and then decreases exponentially with depth due to CaCO3 re-dissolution. The NPZD+Chl ecosystem is coupled to the inorganic/solubility pump via sources/sinks of DIC and TA regulated by sources/sinks

of $CaCO_3$ and N.

Chapter 2

Ocean general circulation model

The ocean model is a developmental version of the ocean component of the Canadian Centre for Climate Modelling and Analysis coupled global climate model (CGCM) (Flato *et al.* 2000). It is a rigid-lid model that derives from the NCAR CSM ocean model (NCOM), which in turn is based on the GFDL MOM v.1.1 ocean model. In this configuration it has 29 levels in the vertical and a uniform horizontal grid of about 1.86° (192x96). The vertical resolution increases toward the ocean surface, from 300 m in the deep ocean to 50 m in the top 200 meters.

Isopycnal mixing and transport is parameterized according to the method of Gent and McWilliams (1990), with thickness and isopycnal diffusion coefficients of 1×10^3 $m^2 s^{-1}$. Vertical mixing within the surface mixed layer is parameterized as vertical diffusion of momentum and tracers with large diffusivity coefficients, solved implicitly. There is also a constant background vertical diffusivity for tracers set to 3×10^{-5} $m^2 s^{-1}$.

Chapter 3

Inorganic chemistry module - solubility pump

The Ocean Carbon Model Intercomparison Project (OCMIP) - phase 2 (http://www.ipsl.jussieu.fr/OCMIP/phase2/) developed a set of protocols in an effort, in part, to standardize the implementation of inorganic chemistry across models from different groups for the purpose of model intercomparison studies. We incorporated the updated version of their inorganic chemistry module, or solubility pump, in our model.

Whenever carbon dioxide enters the ocean, it becomes a dissolved gas $CO_{2(aq)}$. A small part of $CO_{2(aq)}$ becomes hydrated, forming carbonic acid H_2CO_3. The mixture of dissolved gas and carbonic acid partly dissociates to bicarbonate HCO_3^- and carbonate CO_3^{2-} ions until a chemical equilibrium is reached rapidly. The reactions only depend on the sum of the concentrations of $CO_{2(aq)}$ and H_2CO_3, henceforth denoted by $[CO_2^*]$.

3.1 Dissolution of CO_2

According to the modified form of Henry's law (Weiss 1974), the saturation concentration $[CO_2]^{sat}$ of carbon dioxide in a solution in equilibrium with an overlying atmosphere, at total pressure P, is given by the expression

$$[CO_2]^{sat} = K_0 \; f_{CO_2} \; exp[(1 - P) \; \hat{v}/RT] \tag{3.1}$$

where

- K_0, in units of $mol/kg \cdot atm$, is the solubility coefficient for the reaction

$$CO_{2(g)} \rightleftharpoons CO_{2(aq)} \tag{3.2}$$

- f_{CO_2} is fugacity of CO_2, in units of atm
- P is the total pressure, in atm
- $\hat{v}$ is the partial molal volume of CO_2, in L/mol
- R is the gas constant, in $L \cdot atm/K \cdot mol$
- T is the absolute temperature, in K.

The fugacity of the gas, which for an ideal gas is equal to the partial pressure, is given by the expression

$$f_{CO_2} = \chi^{sat}_{CO_2} \; P \times exp\left\{ \int_0^P (\hat{v}/RT - 1/P) \, dp \right\} \tag{3.3}$$

The mole fraction of CO_2 in moist/saturated air, appropriate for the atmosphere-ocean interface, is related to the mole fraction in dry air by

$$\chi^{sat}_{CO_2} = \chi^{dry}_{CO_2} \times (1 - pH_2O/P) = \chi^{dry}_{CO_2} \times (1 - \chi_{H_2O}) \tag{3.4}$$

where pH_2O is the water vapour pressure and χ_{H_2O} is the mole fraction of water vapour.

If we assume that the gas can be represented via a virial expansion of the equation of state as a combination of an ideal gas and a deviation from that, then the integral in (3.3) can be simplified. Using (3.4) we can thus write

$$f_{CO_2} = \chi^{dry}_{CO_2}\ P\ (1 - \chi_{H_2O}) \times exp\left[P\ (B + 2\delta)/RT\right] \tag{3.5}$$

where B is the second virial coefficient for pure CO_2 and δ involves cross-virial coefficients.

Using (3.5), we can re-write (3.1) as

$$[CO_2]^{sat} = \chi^{dry}_{CO_2}\ P \times F_P \tag{3.6}$$

where F_P is

$$F_P = K_0\ (1 - \chi_{H_2O}) \times exp\left[P\ \frac{B + 2\delta}{RT} + (1 - P)\ \frac{\hat{v}}{RT}\right] \tag{3.7}$$

The CO_2 saturation concentration in (3.6) depends on the total pressure — indirectly through the pressure dependence of F_P and directly through P.

3.2 Dissociation of CO_2^*

The flux of carbon dioxide across the air-sea interface is controlled by the difference in the surface concentrations (or equivalent partial pressures) of CO_2 between the

ocean and the atmosphere (Millero 1995). It is calculated as

$$F_{CO_2} = k_w \Delta[CO_2] = k_w \; F_P \; \Delta pCO_2 \tag{3.8}$$

where k_w is piston or gas transfer velocity for CO_2. The magnitude of the exchange depends on the sea state, the presence of sea ice, the ambient sea-surface temperature and salinity, the atmospheric surface pressure, and total alkalinity.

The piston or gas transfer velocity is parameterized as proportional to the square of the 10-meter wind speed, as per Wanninkhof (1992):

$$k_w = a(1 - f_{ice}) U_{10}^2 (Sc^*)^{-1/2} \tag{3.9}$$

where a is a constant of proportionality; f_{ice} is fractional area of model grid square covered by ice; U_{10} is wind speed at 10-m above ocean surface; $Sc^* = (\nu/D)/660 = f(T)$ is the Schmidt number: a ratio of the kinematic viscosity of water ν to the CO_2 gas diffusivity D, normalized to a reference value of 660. The intercept was adjusted to conserve the global mean piston velocity as discussed by Wanninkhof (1992). There is no gas exchange through ice; the ice mask is derived from the CGCM (Flato *et al.* 2000).

The sea-air difference in CO_2 concentration is calculated as

$$\Delta[CO_2] = [CO_2^*] - [CO_2]^{sat} = [CO_2^*] - \chi_{CO_2}^{dry} \; P \times F_P \tag{3.10}$$

and

$$\Delta pCO_2 = pCO_2^{ocn} - pCO_2^{atm} = [CO_2^*]/F_P - \chi_{CO_2}^{dry} \; P \tag{3.11}$$

where $[CO_2^*]$ is calculated as follows.

Dissolved inorganic carbon (DIC) is a sum of the concentrations of the three chemical species in equilibrium, CO_2^*, bicarbonate ion HCO_3^-, and carbonate ion CO_3^{2-}, and it represents a mass conservation equation for inorganic carbon:

$$[DIC] = [CO_2^*] + [HCO_3^-] + [CO_3^{2-}] \tag{3.12}$$

The relative proportions of the species in eq.(3.12) depend on sea-surface temperature, salinity, pressure, and hydrogen ion concentration (pH). Fig. (3.1) shows the variation with pH of carbonic acid, bicarbonate and carbonate ion concentrations.

Total alkalinity (TA) is a sum of 11 species and represents a mass conservation relationship for the hydrogen ion (Dickson 1981) involving proton donor and acceptor species from DIC, total inorganic phosphate P_T, total borate B_T, total silicate Si_T, total sulphate S_T, total fluoride F_T, and the hydroxyl and hydrogen ions (http://www.ipsl.jussieu.fr/OCMIP/phase2/):

$$\begin{aligned} TA &= [HCO_3^-] + 2[CO_3^{2-}] + [B(OH)_4^-] + [OH^-] + [H_3SiO_{4^-}] \\ &\quad + [HPO_4^{2-}] + 2[PO_4^{3-}] - [H_3PO_4] - H_f - [HSO_4^-] - [HF] \end{aligned} \tag{3.13}$$

Total inorganic phosphate P_T and total silicate Si_T are given by surface reference values and are constants for the model. Total borate B_T (Uppström 1974), total sulphate S_T (Morris and Riley 1966), and total fluoride F_T (Riley 1965) are estimated as linear functions of model sea-surface salinity.

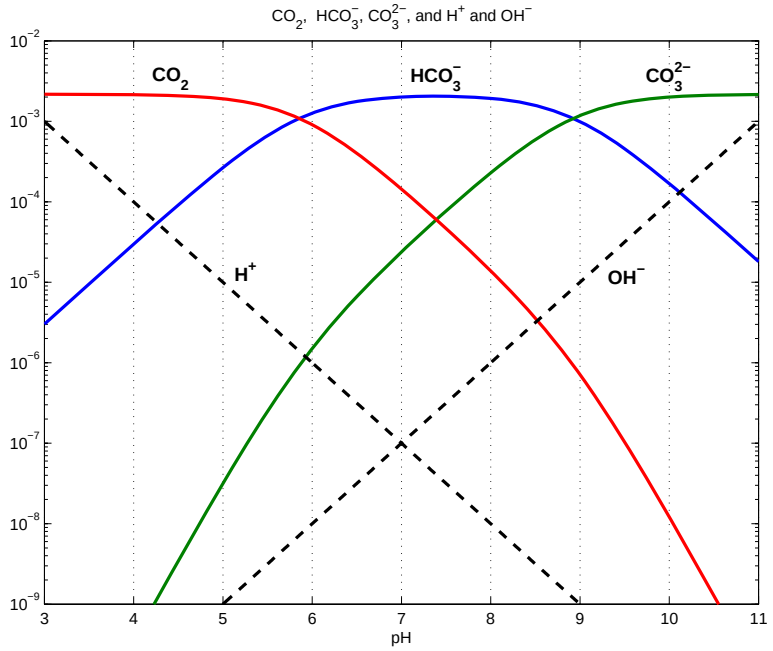

FIG. 3.1. Bjerrum plot of the relative proportions of $[CO_2^*], [HCO_3^-], [CO_3^{2-}]$, and $[H^+]$ and $[OH^-]$, as a function of pH

Given P_T and Si_T, and the model ocean surface salinity (SSS), temperature (SST), DIC and TA, then (i) B_T S_T and F_T are estimated from SSS; (ii) eleven dimensional dissociation constants for the various chemical equilibrium reactions between species are computed via polynomial proxies from SSS and SST; (iii) the TA equation is re-written as the zero of a non-linear function of $[H^+]$ via the algebraic relationships between equilibrium dissociation constants and the chemical species' concentrations in the respective reactions; (iv) surface $[H^+]$ (thus pH) is determined by an iterative solution procedure so that the TA equation is satisfied within the margins of accepted error. Fig. (3.2) shows how pH varies with DIC and TA (left panel) and with SST and SSS (right panel).

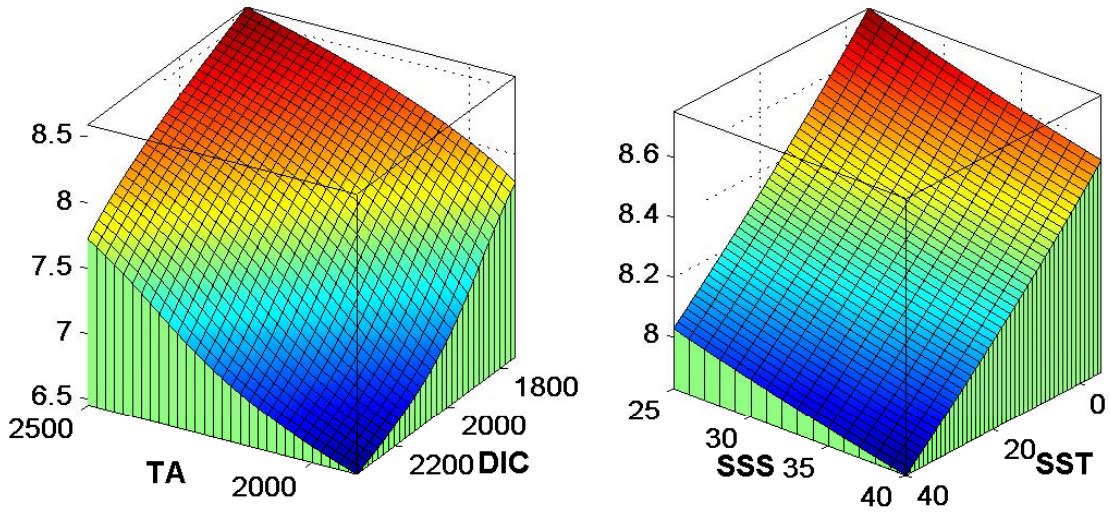

FIG. 3.2. Dependence of pH on dissolved inorganic carbon DIC and total alkalinity TA (left), and on sea-surface temperature SST and salinity SSS (right)

Lastly, surface ocean $[CO_2^*]$ concentration is computed from an equation derived from the mass balance (3.12) for DIC above and the two algebraic equations for the dissociation constants K_1 and K_2 for the $[CO_2^*] \rightleftharpoons [HCO_3^-]$ and $[HCO_3^-] \rightleftharpoons [CO_3^{2-}]$ reactions:

$$[CO_2^*] = \frac{DIC[H^+]^2}{[H^+]^2 + K_1[H^+] + K_1K_2} \tag{3.14}$$

Note that all dissociation constants have a weak dependence on pressure which has been neglected here; thus all polynomial proxies are derived for $P = P_0 = 1atm$.

3.3 The standard pressure approximation for the surface ocean

We assumed that the dissociation constants for the acid-base system in the surface ocean can be approximated, to first order, with polynomial proxies evaluated at a standard pressure of 1 atmosphere. Let us also assume that the generalized solubility coefficient F_P in (3.7) has a similar weak dependence on pressure, at least as compared to the explicit linear pressure dependence of $[CO_2]^{sat}$ in (3.6) . Then F_P is evaluated at a standard pressure $P = P_0 = 1\ atm$,

$$F_{P_0} = K_0\ (1 - pH_2O/P_0) \times exp\left[\frac{B + 2\delta}{RT}\right] \tag{3.15}$$

and

$$[CO_2]^{sat}_{P_0} = \chi^{dry}_{CO_2}\ P\ F_{P_0} \tag{3.16}$$

The expression in (3.15) is fitted by Weiss and Price (1980) to a polynomial of the form

$$ln(F_{P_0}) = A_1 + A_2\ (100/T) + A_3\ ln(T/100) + A_4\ (T/100)^2 + S[B_1 + B_2\ (T/100) + B_3\ (T/100)^2] \tag{3.17}$$

where T is ocean temperature and S is ocean salinity.

Then in place of (3.10) and (3.11) we have

$$\Delta[CO_2]_{P_0} = [CO^*_2]_{P_0} - \chi^{dry}_{CO_2}\ P \times F_{P_0} \tag{3.18}$$

and

$$\Delta pCO_{2\,P_0} = [CO_2^*]_{P_0}/F_{P_0} - \chi^{dry}_{CO_2}\ P \tag{3.19}$$

In the absence of polynomial fits for F_P and having all dissociation constants of the acid-base system in the surface ocean fitted at pressure $P_0 = 1\ atm$[1], we can evaluate (3.18) and (3.19) instead.

[1]Millero (1995) presented a formula for calculating the effect of pressure on equilibrium constants, however the polynomial fits are not given for some species needed here and the rest are fitted for a constant salinity of 35 psi.

Chapter 4

Ecosystem model - organic and carbonate pumps

4.1 Combined equations and coupling between components

An NPZD-type ecosystem model similar to the 1-D model developed by Denman and Peña (1999) was implemented in the global ocean model (Figure 4.1).

There is one class of phytoplankton (P) with a growth rate limited by light, temperature, nitrogen, and iron, one class of zooplankton (Z), and a single nutrient variable (N) that implicitly includes nitrate, ammonium and urea. There is a surface source of N via dinitrogen fixation by diazotrophs. The detritus variable (D) implicitly combines dissolved, suspended and sinking organic matter, with a constant sinking rate. The currency of the model is nitrogen, and the biological effect on DIC is calculated via a constant Redfield C:N ratio. Chlorophyll (Chl) is a separate prognostic variable based on a varying Chl:N ratio. Growth and remineralization rates

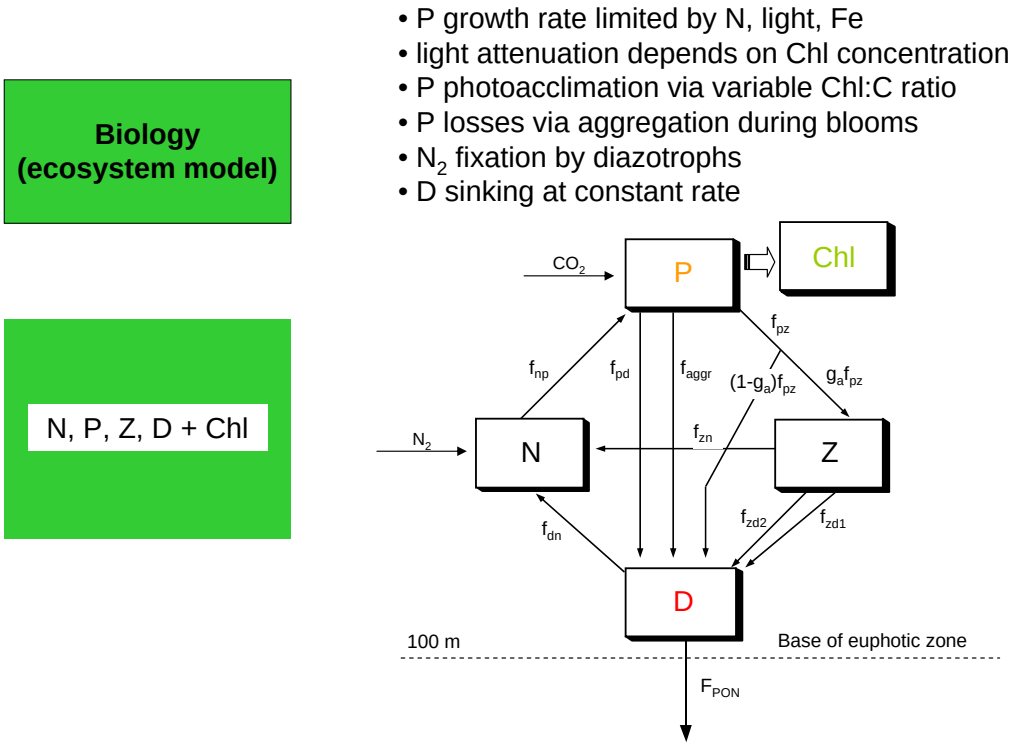

FIG. 4.1. CMOC v.1.0: Organic pump

are temperature-dependent. Production of calcium carbonate by phytoplankton and its dissolution at depth are parameterized, respectively, as a temperature-dependent fraction of particulate organic matter exported from the euphotic zone ('rain ratio') and as an exponentially-decreasing flux ('instantaneous' transport to depth). Model parameter values are listed in Table 1.

The carbon model equations are

$$dDIC/dt = L(DIC) \quad +\partial F^{CO_2}/\partial z + \partial F_v^{DIC}/\partial z \quad +R_{C:N}\, J^{N^*} \quad + \quad J^{CaCO_3} \tag{4.1}$$

$$dTA/dt = L(TA) \quad + \partial F_v^{TA}/\partial z \quad - \quad J^{N^*} \quad +2\, J^{CaCO_3} \tag{4.2}$$

$$dN/dt = L(N) \quad + \partial F_v^{N}/\partial z \quad + \quad J^{N} \tag{4.3}$$

$$dP/dt = L(P) \quad + \partial F_v^{P}/\partial z \quad + \quad J^{P} \tag{4.4}$$

$$dZ/dt = L(Z) \quad + \partial F_v^{Z}/\partial z \quad + \quad J^{Z} \tag{4.5}$$

$$dD/dt = L(D) \quad + \partial F_v^{D}/\partial z \quad + \quad J^{D} \tag{4.6}$$

$$dChl/dt = L(Chl) \quad + \partial F_v^{Chl}/\partial z \quad + \quad J^{Chl} \tag{4.7}$$

where $L(X) = A(X) + D(X)$, where A represents advection (as for temperature and salinity) by the combined fluid and (Gent and McWilliams 1990) 'bolus' velocities via a third-order upwind scheme, D represents isopycnal and diapycnal diffusion as prescribed by the various mixing parameterizations; F_v^X is a surface virtual tracer flux; J^X is an ecosystem model source/sink term as detailed below; F^{CO_2} is the surface flux of carbon dioxide; $J^{N^*} = J^N - J^{Nf}$, where J^{Nf} represents dinitrogen fixation and denitrification; J^{CaCO_3} is a sink for alkalinity in the euphotic zone resulting from export of $CaCO_3$ and a source below the euphotic zone from $CaCO_3$ redissolution, as described below.

The source/sink terms from the ecosystem model are

$$J^N = -\Gamma\, P \quad +m_{zn}\, Z \quad +r_e\, D \quad +J^{Nf} \tag{4.8}$$

$$J^P = \Gamma\, P - \Lambda\, Z \quad -m_{pd}\, P - m_{aggr}\, P^2 \tag{4.9}$$

$$J^Z = g_a \Lambda\, Z \quad -m_{zn}\, Z \quad -m_{zd}\, Z - m_{zd_2}\, Z^2 \tag{4.10}$$

$$J^D = (1-g_a)\Lambda\, Z \quad +m_{pd}\, P + m_{aggr}\, P^2 \quad +m_{zd}\, Z + m_{zd_2}\, Z^2 \quad -r_e\, D \quad +w_s\, \partial D/\partial z \tag{4.11}$$

$$J^{Chl} = \theta^N\, J^P \quad +(\theta^N_{bal} - \theta^N)\, P/\tau_\theta \tag{4.12}$$

Phytoplankton growth rate Γ is determined by light, temperature, nitrogen, and iron, and is calculated as a temperature-dependent maximum growth rate times the minimum of three nondimensional limitation functions (Fig. 4.2)

$$\Gamma(I_{PAR}, \theta, N, Fe) = v_m\; min\left\{ \left[1 - exp(-\alpha_{Chl}\theta I_{PAR}/v_m)\right], \frac{N}{N + K_N}, L_{Fe} \right\} \tag{4.13}$$

where I_{PAR} is photosynthetically active radiation (PAR), and θ is the $Chl:C$ ratio.

Phytoplankton are grazed by zooplankton at a rate Λ (Fig. 4.3) calculated as

$$\Lambda(P) = r_m \frac{P^2}{P^2 + {K_P}^2} \tag{4.14}$$

and zooplankton is assumed to utilize a fraction g_a of that, the rest, a source of Detritus, attributed to "messy feeding".

Phytoplankton senescense losses are represented as linear in P. Phytoplankton mortality also occurs through aggregation, parameterized as quadratic in P so that

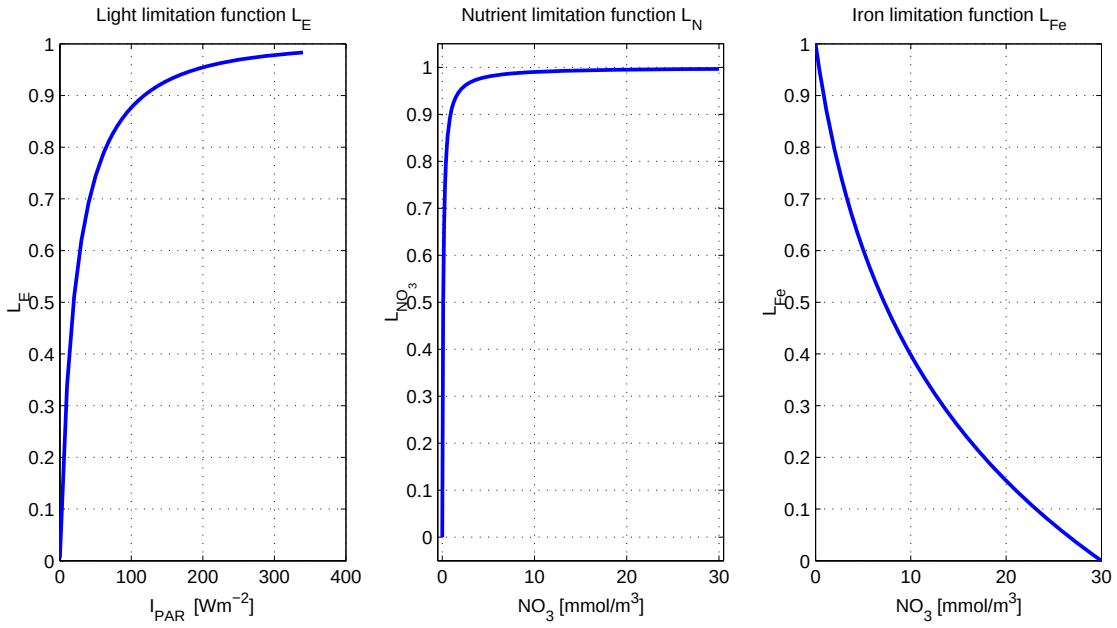

FIG. 4.2. Phytoplankton growth limiting functions: light limitation (left), nutrient limitation (centre), iron limitation (right)

it is significant only when phytoplankton "blooms". The model is closed via linear and quadratic mortality terms for zooplankton implying predation by an uynresolved higher trophic level. The nonlinear term was added because it stabilizes the model at extreme zooplankton concentrations (Steele and Henderson 1992; McCreary *et al.* 1996). Zooplankton respiration is represented by a linear loss term from Z to N.

Remineralization of detritus is linear in D with a temperature-dependent rate coefficient. Detritus sinks with a constant speed w_s. This results in an export flux of nitrogen from the euphotic zone $F_{PON} = w_s D_i$ where i is the index of the last model layer within the euphotic zone. The euphotic zone depth is fixed at 100 m (Table

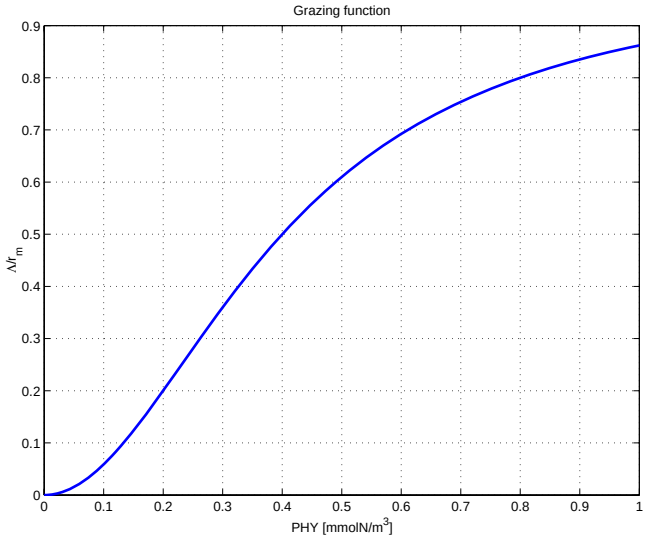

FIG. 4.3. Grazing of phytoplankton by zooplankton: grazing rate function

1). Because detrital remineralization is temperature-dependent, the remineralization length scale w_s/r_e will generally increase with depth.

The solubility, organic and carbonate pumps are coupled and also change the physical environment through ocean temperature. Dissolved inorganic carbon is affected by carbon uptake and remineralization and by $CaCO_3$ precipitation and re-dissolution. Total alkalinity is affected by nitrogen uptake and remineralization (through changes in OH^- and H^+ concentrations) and by carbonate precipitation and re-dissolution at depth. Chlorophyll biomass affects the vertical distribution of heat in the physical model through changes in light attenuation.

4.2 Light and photosynthesis

The photosynthetically-active fraction I_{PAR} of the solar radiative flux $I^0(t)$ that enters the surface ocean is attenuated with depth using a single exponential formulation

$$I_{PAR}(z,t) = a_{par} \times I_m^0 \; g(t) \times exp\{-k(Chl)\; z\} \tag{4.15}$$

where a_{par} is the fraction of the irradiance that is in the photosynthetically-active band, I_m^0 is the local noon maximum irradiance, $g(t)$ represents the normalized temporal variation of the irradiance within a diel cycle, and Chl is chlorophyll concentration. We set $a_{par} = 0.45$ (Baker and Frouin 1987). The remaining fraction $(1 - a_{par}) \times I^0(t)$ would correspond to a longer wavelength band; it is assumed to have been absorbed within the first model layer due to its very short attenuation depth.

The total attenuation coefficient k varies linearly with chlorophyll (Spitz *et al.* 2001; Moore *et al.* 2002; Lima and Doney 2004)

$$k = k_w + k_{Chl} Chl \tag{4.16}$$

where k_w is PAR attenuation coefficient for phytoplankton-free seawater, and k_{Chl} is PAR attenuation coefficient for chlorophyll (Table 1). The typical range for k is between 0.04 m^{-1} and 0.08 m^{-1}, corresponding to attenuation depths between 12 and 25 metres.

The photosynthesis-light relationship, without photoinhibition, is that of Platt et

al. (1980):

$$\Pi^B(z,t) = P_m^B \left[1 - exp(-\alpha_{Chl} I_{PAR}/P_m^B)\right] \tag{4.17}$$

where Π^B is chlorophyll-specific primary production rate, P_m^B is the assimilation number – a chlorophyll-specific primary production rate at saturating light, α_{Chl} is a chlorophyll-normalized initial slope which is assumed constant (Geider *et al.* 1997; Geider *et al.* 1998; MacIntyre *et al.* 2002; Behrenfeld *et al.* 2004).

The corresponding nitrogen-specific primary production rate can be expressed as

$$\Pi^N(z,t) = v_m \left[1 - exp(-\alpha_{Chl}\theta I_{PAR}/v_m)\right] = v_m \left[1 - exp(-\alpha I_{PAR}/v_m)\right] \tag{4.18}$$

where v_m and the initial slope α are related to P_m^B and α_{Chl}, respectively, via the variable $Chl:C$ ratio θ:

$$\alpha = \alpha_{Chl}\theta \tag{4.19}$$

$$P_m^B = v_m/\theta \tag{4.20}$$

4.3 Temperature dependence of coefficients

We assume that ambient temperature affects phytoplankton physiology by limiting the maximum photosynthesis rate v_m (Eppley 1972; Li and Dickie 1987; Lefévre *et al.* 2003). We use an Arrhenius equation (Li 1980; Raven and Geider 1987; Arrhenius 1889) for the temperature dependence of v_m (Geider *et al.* 1997; Geider *et al.* 1998; Flynn 2001; Moore *et al.* 2002)

$$v_m = v_m^{ref} \times exp\left[\frac{-E_P}{R}\left(\frac{1}{T} - \frac{1}{T_{ref}^{v_m}}\right)\right] \tag{4.21}$$

where v_m^{ref} is a reference maximum photosynthesis rate at a temperature $T_{ref}^{v_m}$, E_P is the activation energy for growth, and R is the universal gas constant (Fig. 4.4).

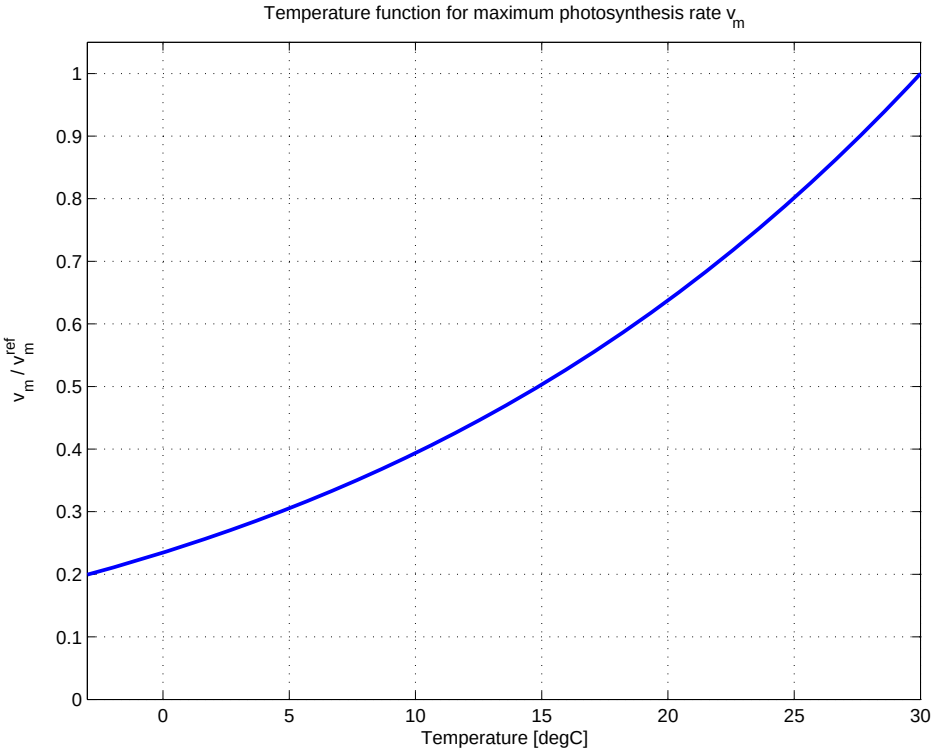

FIG. 4.4. Temperature dependence of the maximum photosynthetic rate v_m

We model the temperature dependence of the remineralization rate r_e (Li and Dickie 1987) using the same temperature function but with a higher activation energy than for growth (Li and Dickie 1987; Rivkin and Legendre 2001)

$$r_e = r_e^{ref} \times exp\left[\frac{-E_D}{R}\left(\frac{1}{T} - \frac{1}{T_{ref}^{v_m}}\right)\right] \tag{4.22}$$

where r_e^{ref} is a reference maximum remineralization rate at a temperature $T_{ref}^{v_m}$, and E_P is the activation energy for remineralization.

4.4 Primary production integrals

The ecosystem module is embedded in a physical model with four 50-metre layers in the first 200 metres near the ocean surface. In order to determine the appropriate phytoplankton growth rate and daily primary production we used the integration over depth and daily cycle of Platt *et al.* (1990; 1991), originally developed for calculating the daily water column primary production, then extended for an arbitrary layer (Platt and Sathyendranath 1993). Since the ocean carbon model is run for thousands of model years to achieve carbon equilibrium, this formulation allows the use of a daily time-step while accurately calculating daily primary production by taking into account the non-linearities in the response of phytoplankton to the diel cycle of irradiance. In coupled mode, however, the ocean carbon model resolves the diel cycle of irradiance. We present the corresponding analytical depth integrals of primary productivity for a diel-resolving time-step.

4.4.1 Analytical daily integral without resolving the diel cycle

We assume that the diel variation of surface irradiance can be represented sufficiently well by a sine function (Kirk 1994; Harris 1980) so that

$$g(t) = sin(\pi t/d_D) \tag{4.23}$$

where $d_D < 24$ is daylength in hours. We will consider the special case of a polar day ($d_D = 24$ hours) in the next subsection.

Rewriting (4.18) to explicitly show the time and depth dependence of I_{PAR} from (4.15), we have

$$\Pi^N(z,t) = v_m \left[1 - exp\left(-\alpha_{Chl}\theta \times a_{par} I_m^0 \; sin(\pi t/d_D) \times exp\left\{-k(Chl)\; z\right\}/v_m\right)\right] \tag{4.24}$$

In the absence of nutrient and iron limitation, the daily primary production would be

$$\Pi_{Z,T}^N = \iint P \times \Pi^N(z,t)\; dz\; dt \tag{4.25}$$

Assuming that P, k, and θ are constant with depth and within the model time-step (they could vary across model layers and only need to be constant within each model layer, as shown later), we have

$$\Pi_{Z,T}^N = P v_m \int_{t=0}^{d_D} \int_{z=0}^{\infty} \left[1 - exp\left(-\alpha_{Chl}\theta \times a_{par} I_m^0 \; sin(\pi t/d_D) \times e^{-k\, z}/v_m\right)\right] \; dz\; dt \tag{4.26}$$

Following Platt *et al.* (1990) we define the nondimensional irradiance

$$I_*^m = a_{par} I_m^0 (\alpha_{Chl}\theta/v_m) = a_{par} I_m^0 / I_k \tag{4.27}$$

where $I_k = P_m^B/\alpha_{Chl}$ is the photoadaptation parameter.

Let

$$u = I_*^m \; sin(\pi t/d_D) \times e^{-k\,z} \tag{4.28}$$

and consequently

$$\Pi_{Z,T}^N = \frac{P v_m}{k} \int_{t=0}^{d_D} \left\{ \int_{z=0}^{I_*^m \; sin(\pi t/d_D)} \frac{1 - e^{-u}}{u} \; du \right\} \; dt \tag{4.29}$$

The integral in the curly brackets is the Ein function, an exponential integral of the form

$$Ein(x) = \int_{z=0}^{x} \frac{1 - e^{-u}}{u} \; du \tag{4.30}$$

with a series expansion

$$Ein(x) = \sum_{n=1}^{\infty} \frac{(-1)^{n+1}}{n \cdot n!} \; x^n \tag{4.31}$$

Making the change of variable

$$\vartheta = \pi t/d_D \tag{4.32}$$

eq. (4.29) becomes

$$\Pi_{Z,T}^N = \frac{P v_m d_D}{k} \int_{\vartheta=0}^{\pi} \sum_{n=1}^{\infty} \frac{(-1)^{n+1}}{\pi \; n \cdot n!} \; (I_*^m \; sin\vartheta)^n \; d\vartheta \tag{4.33}$$

Repeated application of the identity

$$\int_0^{\pi} sin^n\vartheta \; d\vartheta = n^{-1} \; (n-1) \int_0^{\pi} sin^{n-2}\vartheta \; d\vartheta \tag{4.34}$$

leads to an analytical solution of the form

$$\Pi^N_{Z,T} = A \times f(I^m_*) \tag{4.35}$$

where $A = Pv_m d_D/k$ is a scale factor.

The nondimensional function $f(I^m_*)$ is an infinite series which is approximated very well by a fifth-degree polynomial of I^m_* so that

$$\Pi^N_{Z,T} = A \times \sum_{x=1}^{5} \Omega_x (I^m_*)^x \tag{4.36}$$

and the weights Ω_x are given by Platt *et al.* (1993).

This expression is then generalized for an arbitrary model layer n of thickness Δz_n, extending from $z = z_{n-1}$ to $z = z_n$, with phytoplankton nitrogen P_n and an attenuation coefficient k_n as follows:

$$\Pi^N_{\Delta z_n,T} = A_n \times \left\{ f\left(I^m_* exp(-\sum_{p=1}^{n-1} k_p \Delta z_p) \right) - f\left(I^m_* exp(-\sum_{p=1}^{n} k_p \Delta z_p) \right) \right\} \tag{4.37}$$

where $A_n = P_n v_m d_D/k_n$.

The corresponding daily primary production rate per unit volume is

$${}^{P_n}\Pi^N_{\Delta z_n,T} = \Pi_{\Delta z_n,T}/(P_n \Delta z_n) \tag{4.38}$$

4.4.2 Analytical integral within a resolved diel cycle

If the time step in a numerical model is small enough so that the diel cycle of surface irradiance is resolved, calculating the rate of primary production per time-step, $\Pi^N_{Z,\Delta t}$, still involves an integration over the model (layer) depth.

In 1-D mixed models the integration is typically approximated by calculating the average irradiance or the irradiance at mid-depth, for each model layer. This is justified in most cases since the typical vertical resolution in those models is of the order of a metre. In our global carbon model, however, the best vertical resolution near the surface is 50 metres. We therefore proceed with the calculation of the vertical integral of (4.18), for a given surface irradiance $I^0_{\Delta t}$ within a diel-resolving time-step Δt.

We define nondimensional irradiance for a given time-step as

$$I^{\Delta t}_* = a_{par} I^0_{\Delta t} / I_k \tag{4.39}$$

Let

$$u = I^{\Delta t}_* \times e^{-k\,z} \tag{4.40}$$

and consequently

$$\Pi^N_{Z,\Delta t} = \frac{P v_m}{k} \int_{z=0}^{I^{\Delta t}_*} \frac{1 - e^{-u}}{u}\, du \times \Delta t \tag{4.41}$$

Given (4.30), this can be expressed via the Ein function as

$$\Pi^N_{Z,\Delta t} = \frac{P v_m}{k} Ein\left(I^{\Delta t}_*\right) \times \Delta t \tag{4.42}$$

The *Ein* function can be approximated by a fifth-degree polynomial (Abramowitz and Stegun 1965) so that

$$\Pi^N_{Z,\Delta t} = A^{\Delta t} \times \sum_{x=1}^{5} \Omega_x^{\Delta t} (I_*^{\Delta t})^x \tag{4.43}$$

where $A^{\Delta t} = P v_m \Delta t / k$ and the weights $\Omega_x^{\Delta t}$ are given in Abramowitz and Stegun (1965).

This expression is then generalized for an arbitrary model layer n of thickness Δz_n, extending from $z = z_{n-1}$ to $z = z_n$, with phytoplankton nitrogen P_n and an attenuation coefficient k_n as follows:

$$\Pi^N_{\Delta z_n,\Delta t} = A_n^{\Delta t} \times \left\{ f\left(I_*^{\Delta t} exp(-\sum_{p=1}^{n-1} k_p \Delta z_p) \right) - f\left(I_*^{\Delta t} exp(-\sum_{p=1}^{n} k_p \Delta z_p) \right) \right\} \tag{4.44}$$

where $A_n^{\Delta t} = P_n v_m \Delta t / k_n$.

The corresponding primary production rate per unit volume is

$${}^{P_n}\Pi^N_{\Delta z_n,\Delta t} = \Pi_{\Delta z_n,\Delta t} / (P_n \Delta z_n) \tag{4.45}$$

4.4.3 Analytical integral for a polar day within a resolved diel cycle

Poleward of the Arctic and Antarctic circles, there are times of the year when the surface irradiance varies between a maximum value and a minimum non-zero value.

In the extreme case, at the poles during a polar day the sun's elevation is constant throughout the day.

We will then model the diel variation of surface irradiance as

$$I_{PAR}(t) = a_{par} \times \left\{ I^0_{ms}\ sin(\pi t/d_D) + I^0_c \right\} \tag{4.46}$$

where

$$I^0_c = sin\delta\ sin\lambda - cos\delta\ cos\lambda \tag{4.47}$$

and

$$I^0_{ms} = 2\left(sin\delta - I^0_c\right) \tag{4.48}$$

where δ is the sun's declination and λ is the latitude.

The daily primary production integral is

$$\Pi^N_{Z,T} = Pv_m \int_{t=0}^{d_D} \int_{z=0}^{\infty} \left[1 - exp\left(-\alpha_{Chl}\theta \times a_{par} \times \left\{ I^0_{ms}\ sin(\pi t/d_D) + I^0_c \right\} \times e^{-k\,z}/v_m\right)\right]\ dz\ dt \tag{4.49}$$

We define the nondimensional irradiance as

$$I^{ms}_* = a_{par} I^0_{ms}/I_k \tag{4.50}$$

and

$$I^c_* = a_{par} I^0_c/I_k \tag{4.51}$$

Let

$$u = \{I_*^{ms}\ sin(\pi t/d_D) + I_*^c\} \times e^{-k\,z} \tag{4.52}$$

and consequently

$$\Pi_{Z,T}^N = \frac{Pv_m}{k} \int_{t=0}^{d_D} Ein(I_*^{ms}\ sin(\pi t/d_D) + I_*^c)\ dt \tag{4.53}$$

For a diel-resolving time-step Δt this reduces to a summation over quantities

$$\Pi_{Z,\Delta t}^N = \frac{Pv_m}{k} Ein\left(I_*^{\Delta t}\right) \times \Delta t \tag{4.54}$$

as in (4.42).

4.5 Phytoplankton photoacclimation

Photoacclimation by phytoplankton is modeled via a variable $Chl : C$ ratio. Chlorophyll production is assumed to be proportional to P cell growth with a ratio that varies with recent light conditions. The maximum ratio occurs under low light, reflecting the presumed need for phytoplankton to maximize their photosynthetic efficiency (Kana and Glibert 1987; Geider *et al.* 1996).

Using a constant Redfield ratio $R_{C:N}$, we calculate the source/sink of chlorophyll as the product of the source/sink of phytoplankton nitrogen J^P and the $Chl : P$ ratio θ^N; this is modified by a term that nudges towards a "balanced-growth" $Chl : P$ ratio θ_{bal}^N with a restoring time-scale τ_θ, as done by others (Christian *et al.* 2002).

The balanced-growth $Chl:P$ ratio θ^N_{bal} (Geider *et al.* 1996; Geider *et al.* 1997) is calculated following the linearized approach of Geider *et al.* (1997). Following Geider *et al.* (1997), let

$$\begin{aligned} dP/dt &= P^N P - r^N P & (4.55)\\ dChl/dt &= \left\{\rho^B_{Chl} \times (P^N P) - \theta \times (r^N P)\right\} \times (M_C\, R_{C:N}) & (4.56) \end{aligned}$$

and via $\theta = Chl:C$:

$$dChl/dt = \{P d\theta/dt + \theta dP/dt\} \times (M_C\, R_{C:N}) \quad (4.57)$$

where

$$\rho^B_{Chl} = \theta_m \times P^N/(\alpha_{Chl}\theta I_{PAR}(z,t)) \quad (4.58)$$

is the instantaneous ratio of chlorophyll synthesis to carbon fixation. It is at its maximum ${}^{max}\rho^B_{Chl} = \theta_m$ under low irradiance, where photosynthesis becomes linearly-proportional to light absorption (see (4.18)) and declines as irradiance increases and dP^N/dI_{PAR} decreases as P^N approaches the asymptotic limit v_m (Figure 4.5, lower panel).

Under conditions of balanced growth, by definition, $d\theta/dt = 0$ with $\theta = \theta_{bal}$ and therefore from (4.57) $dChl/dt = \theta_{bal} dP/dt \times (M_C\, R_{C:N})$. It follows via (4.56) that $\theta_{bal} = {}^{bal}\rho^B_{Chl}$. Since

$$\begin{aligned} P^N_{bal} &= v_m[1 - exp(-\alpha_{Chl}\theta_{bal} I_{PAR}(z)/v_m)] & (4.59)\\ {}^{bal}\rho^B_{Chl} &= \theta_m \times P^N_{bal}/(\alpha_{Chl}\theta_{bal} I_{PAR}(z)) & (4.60) \end{aligned}$$

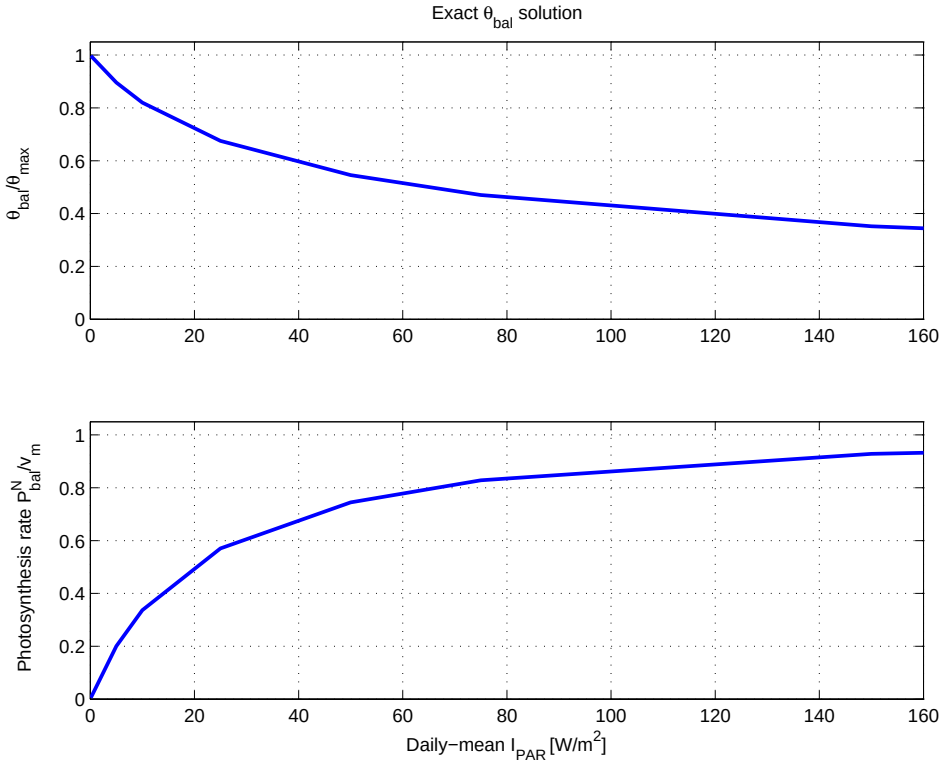

FIG. 4.5. Dependence of $Chl:C$ ratio and growth rate on PAR irradiance under conditions of balanced growth - *exact* solution. Upper panel: normalized $Chl:C$ ratio θ_{bal}/θ_m; Lower panel: normalized rate of phtosynthesis P^N_{bal}/v_m.

then

$$\theta_{bal} = \theta_m \times \frac{[1 - exp(-\alpha_{Chl}\theta_{bal}I_{PAR}(z)/v_m)]}{(\alpha_{Chl}\theta_{bal}I_{PAR}(z)/v_m)} \tag{4.61}$$

Figure 4.5 shows the normalized balanced growth rate P^N_{bal}/v_m (4.59) and the normalized balanced ratio θ_{bal}/θ_m (4.61) as functions of I_{PAR}.

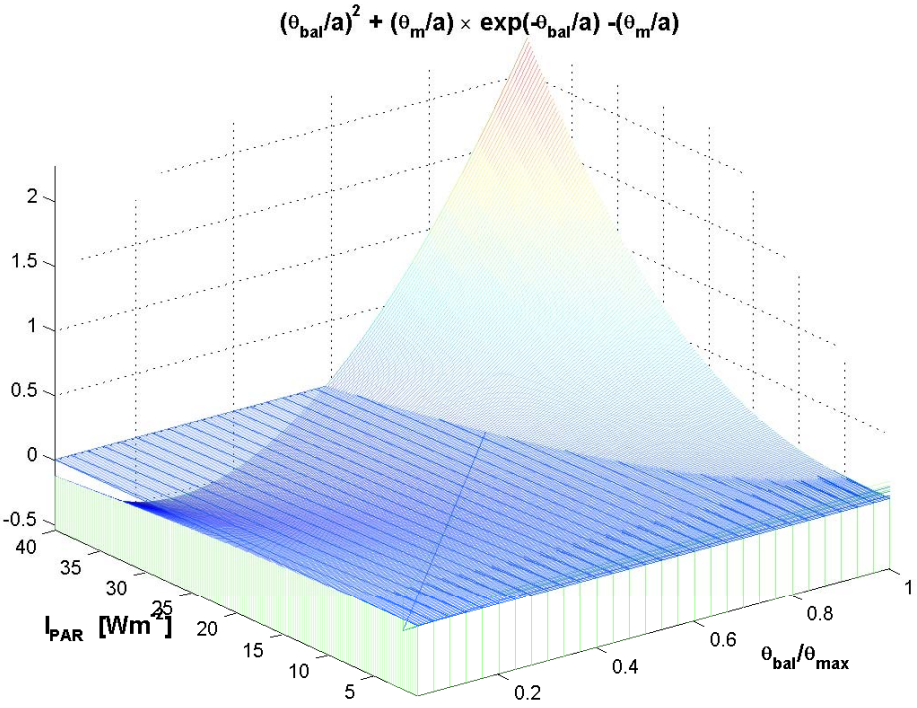

FIG. 4.6. Graphical 3-D representation of the function in equation (4.63) whose zero-crossing of the $I_{PAR}, \theta_{bal}/\theta_m$ plane traces the exact solution for θ_{bal}/θ_m as a function of PAR irradiance.

Let $a = v_m/(\alpha_{Chl} I_{PAR}(z))$. For a given daily-mean, layer-averaged irradiance, and depth, a is a constant, and (4.61) can be written as

$$\theta_{bal} = \theta_m \times \frac{1 - exp(-\theta_{bal}/a)}{(\theta_{bal}/a)} \tag{4.62}$$

or

$$(\theta_{bal}/a)^2 + (\theta_m/a) \times exp(-\theta_{bal}/a) - (\theta_m/a) = 0 \tag{4.63}$$

Equation (4.63) is transcendental and has a well-defined solution (see in Fig. 4.6

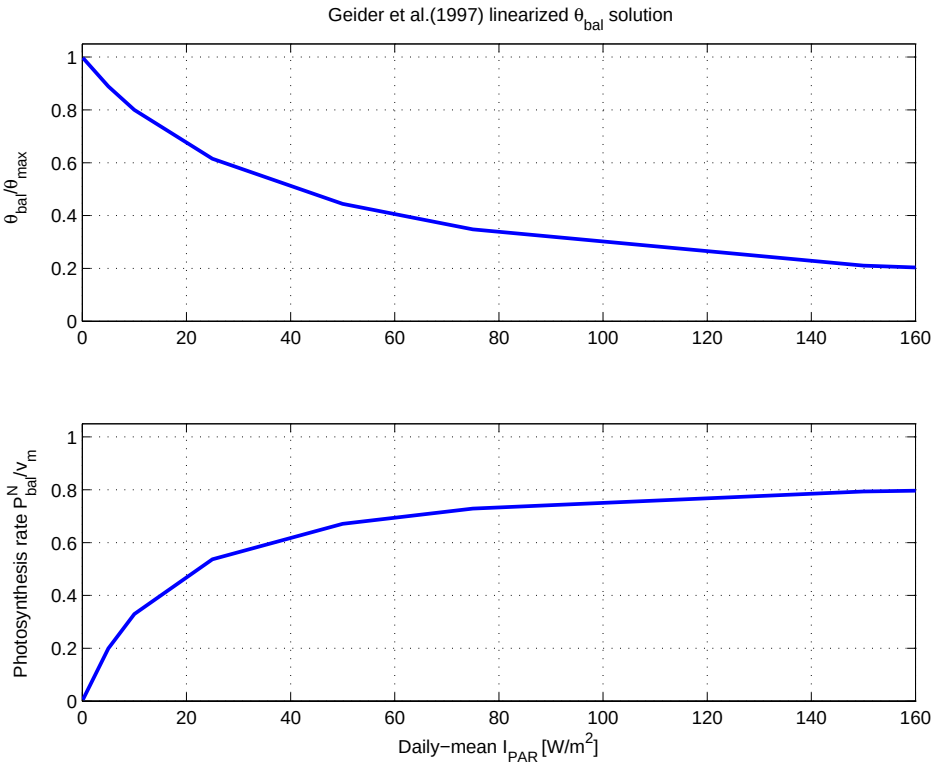

FIG. 4.7. Dependence of $Chl:C$ ratio and growth rate on PAR irradiance under conditions of balanced growth - *linearized* solution (Geider et al. (1997)). Upper panel: Normalized $Chl:C$ ratio θ_{bal}/θ_m; Lower panel: Normalized rate of photosynthesis P^N_{bal}/v_m.

the zero-crossing of the function on the left-hand side of (4.63)).

We can expand (4.62) in Taylor series around $(-\theta_{bal}/a)$:

$$\theta_{bal} = \theta_m \times [1 - \frac{(\theta_{bal}/a)}{2} + \frac{(\theta_{bal}/a)^2}{6} + \cdots] \tag{4.64}$$

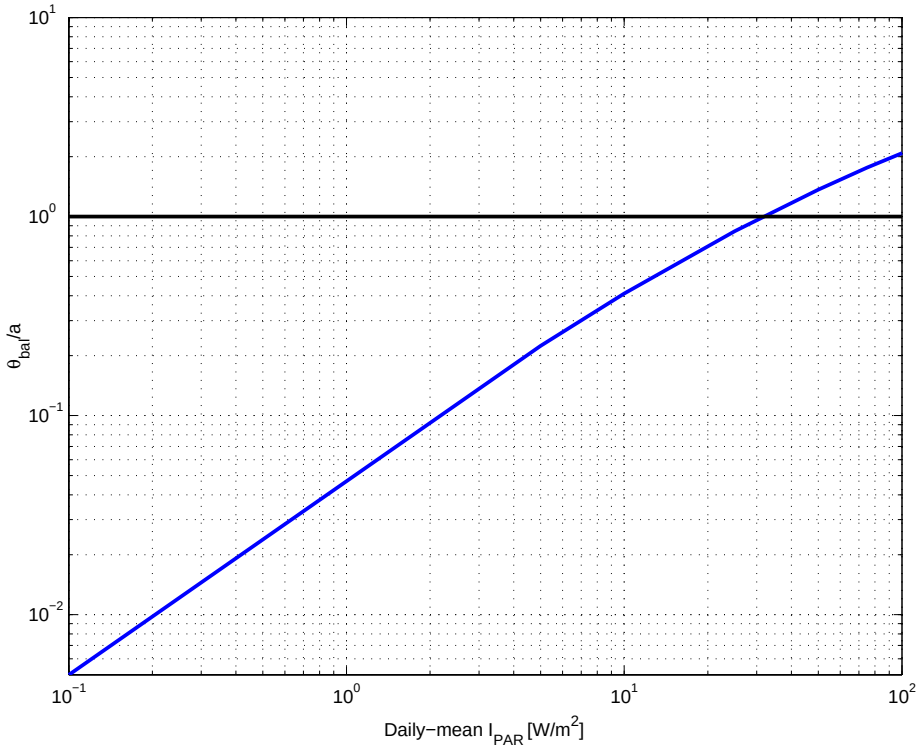

FIG. 4.8. The validity of using a truncated solution for θ_{bal} requires that I_{PAR} is less than 30 Wm^{-2}. The black line denotes $(\theta_{bal}/a) = 1$.

Geider et al. (1997) assumed $\theta_{bal} \lll a$ and linearized (4.64) by truncating the series at the second term and solving for θ_{bal}. After substituting for a, the result is

$$\theta^N_{bal} = M_C \, R_{C:N} \, \theta_m \; / \left(1 + \frac{\alpha_{Chl} \theta_m I_{PAR}}{2 v_m} \right) \tag{4.65}$$

Figure 4.7 shows the resulting normalized balanced growth rate P^N_{bal}/v_m and normalized balanced ratio θ_{bal}/θ_m (4.65) as functions of I_{PAR}.

Compared to the exact solution, the linearized version systematically underestimates θ_{bal} at higher irradiances.

The linearized solution is valid for $\theta_{bal} \lll a$ which implies

$$\theta_{bal} \lll v_m/(\alpha_{Chl} I_{PAR}(z)) \tag{4.66}$$

Depending on the values of the parameters v_m and α_{Chl}, (4.66) cannot be satisfied for irradiances higher than a certain value. As an example, taking $v_m = 3.0\ d^{-1}$ and $\alpha_{Chl} = 5.0\ gCgChl^{-1}d^{-1}(Wm^{-2})^{-1}$, Fig. 4.8 shows that $\theta_{bal} \leq v_m/(\alpha_{Chl} I_{PAR}(z))$ for $I_{PAR} \leq 30\ Wm^{-2}$.

The linear approximation for θ_{bal} is not strictly valid for moderate or large I_{PAR}, although Geider et al. (1997), *ex post facto*, justified the validity of the linearized solution for θ_{bal} even under high irradiances. In our model the vertical resolution is low enough, however, that the layer-averaged daily-mean PAR irradiance is not grossly outside the region of validity for (4.65) even in the top layer.

4.6 Carbonate pump

Calcium carbonate is produced by some species of phytoplankton within the euphotic zone(Fig. 4.9) and exported along with organic carbon. The ratio of inorganic to organic particulate carbon exported from the euphotic zone is termed the 'rain ratio'. The export flux of $CaCO_3$ is:

$$F_{CaCO_3} = R_{C:N}\ R_{Ci:Co}(T)\ F_{PON} \tag{4.67}$$

where the rain ratio $R_{Ci:Co}(T)$ varies with temperature as (Drange 1994)

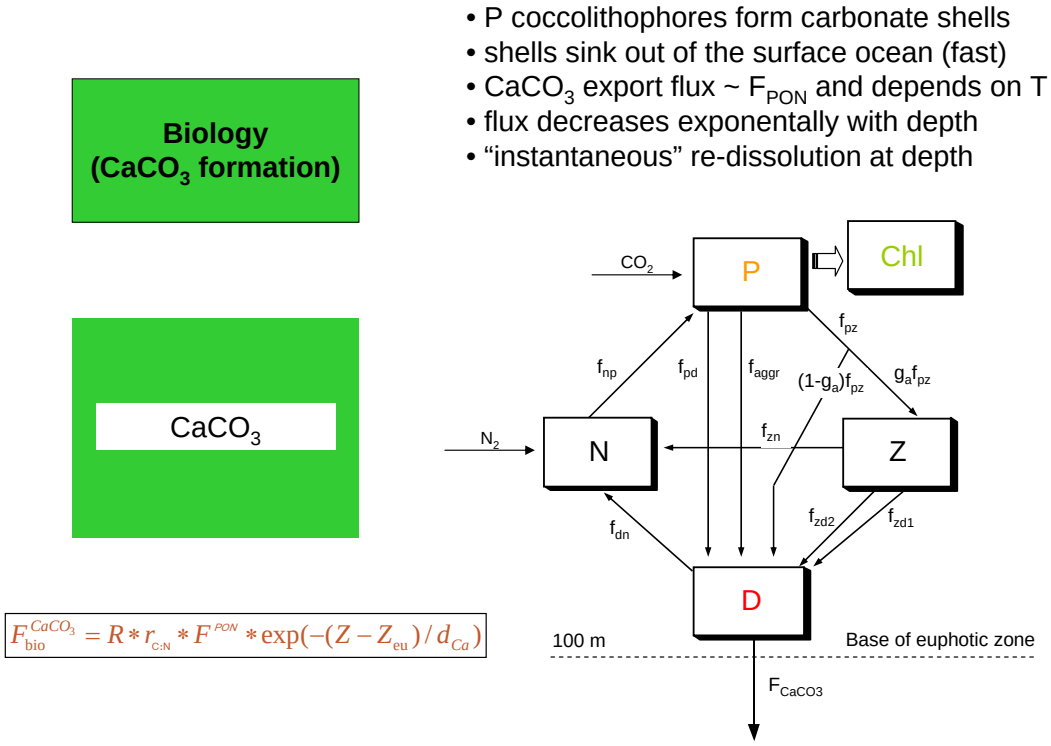

FIG. 4.9. CMOC v.1.0: Carbonate pump

$$R_{Ci:Co}(T) = R^m_{Ci:Co} \times \frac{exp\{a_{Ci}(T - T^r_{Ci})\}}{1 + exp\{a_{Ci}(T - T^r_{Ci})\}} \tag{4.68}$$

and $R_{Ci:Co}(T)/R^m_{Ci:Co}$ is shown on Fig.(4.10). Iglesias-Rodriguez *et al.* (2002) show a similar variability of the $CaCO_3$ flux with ocean temperature.

We model the redissolution of calcium carbonate at depth as 'instantaneous', with the flux decreasing exponentially with depth with a length scale d_{Ci}. Differentiating

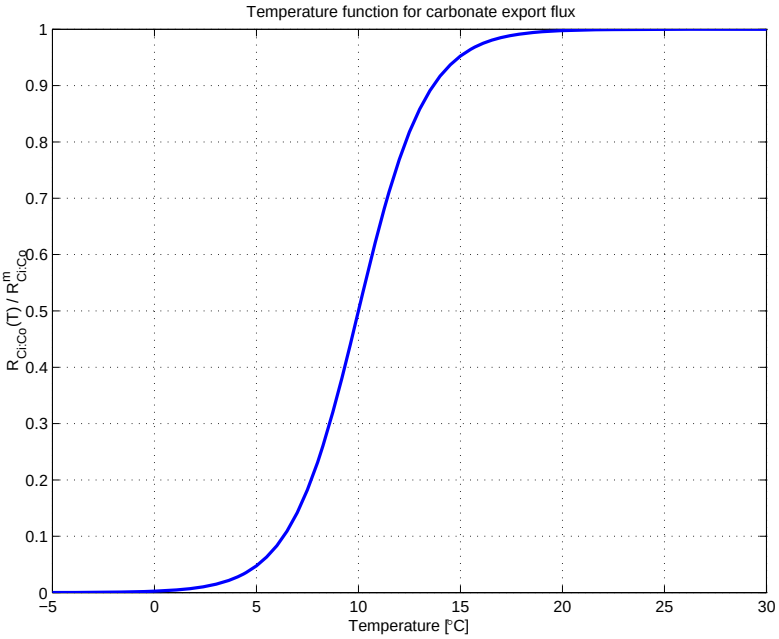

FIG. 4.10. The carbonate export flux is a temperature-varying proportion of the export flux of PON

with respect to depth yields a sink term for calcium carbonate below the depth of the euphotic zone d_{eu},

$$\begin{aligned} J^{CaCO_3} &= -R_{C:N}\ R_{Ci:Co}(T)\ F_{PON} \\ &\quad \times d_{Ci}^{-1}\ exp\left[\frac{-(z-d_{eu})}{d_{Ci}}\right]. \end{aligned} \tag{4.69}$$

The remaining flux of $CaCO_3$ into the sediments is compensated by an equal input at the ocean surface at each grid point so that the global total is conserved. This input may be considered as representing riverine input of $CaCO_3$.

4.7 Nitrogen fixation and denitrification

Nitrogen fixation by diazotrophic bacteria like *Trichodesmium* cyanobacteria in the warm surface waters of the tropical and subtropical oceans represents a source of 'new' N. The subsequent export of organic carbon from the euphotic zone may be important for the global C and N budgets and in terms of affecting the net uptake of atmospheric CO_2 by the ocean (Capone *et al.* 1997). We have implemented a parameterization of dinitrogen fixation, modified from Bissett *et al.* (1999), as a function of sea-surface temperature, light and nutrient availability.

We assume dinitrogen fixation $F_{Nf}(t)$ occurs only in the top 50-m layer. Vertical gradients in irradiance $E(z)$ and diazotroph concentration $\Phi(z)$ are parameterized within the layer. The depth distribution of diazotrophs within the top layer is

$$\Phi(z) = \Phi_{ref}^{Nf}(e\ a_{Nf})\ z\, e^{-a_{Nf} z} + \Phi_0 \tag{4.70}$$

where a_{Nf} is the inverse scale depth of the diazotroph concentration maximum, Φ_0 is the surface reference concentration (trichomes L^{-1}), and Φ_{ref}^{Nf} is the maximum reference concentration of diazotrophs. Following Bissett *et al.* (1999), we scale diazotroph concentration for the layer with sea-surface temperature

$$\Phi(z,T) = \Phi(z) \left(\frac{T - T_{min}^{Nf}}{T_{max}^{Nf} - T_{min}^{Nf}} \right) \tag{4.71}$$

The rate of dinitrogen fixation P^{Nf} is linearly dependent on the surface irradiance

$I_{PAR}(0)$ (Orcutt *et al.* 2001)

$$P^{Nf}(z) = P^{Nf}_{ref}\ \frac{I_{PAR}(0)}{I^{Nf}_{max}}\ e^{-kz} \tag{4.72}$$

where k is the attenuation coefficient (see above section 4.2). We also assume that the N concentration has a limiting role, as other phytoplankton would outcompete the diazotrophs for P and Fe when there is sufficient N (Capone *et al.* 1997). The dinitrogen fixation source term is then

$$J^{Nf}(z) = \frac{K_N}{N + K_N}\ \Phi(z,T)\ P^{Nf}(z) \tag{4.73}$$

Typical depth distributions for diazotroph concentration $\Phi(z)$ and dinitrogen fixation source term J^{Nf} within the top layer are shown in Fig. 4.11.

For a surface layer of thickness Δz_1, the layer-integrated dinitrogen fixation is

$$F_{Nf} = P^{Nf}_{ref}\ \frac{I_{PAR}(0)}{I^{Nf}_{max}}\ \frac{T - T^{Nf}_{min}}{T^{Nf}_{max} - T^{Nf}_{min}}\ \frac{K_N}{N + K_N}\ \left\{ \Phi^{Nf}_{ref}(e\ a_{Nf}) \int_0^{\Delta z_1} z\, e^{-(a_{Nf}+k)\,z} \mathrm{d}z + \Phi_0 \int_0^{\Delta z_1} e^{-k\,z} \mathrm{d}z \right\} \tag{4.74}$$

which is solved analytically since

$$\int_0^{\Delta z_1} z\, e^{-(a+k)\,z} \mathrm{d}z = \frac{1}{(a+k)^2} \left\{ 1 - [(a+k)\Delta z_1 + 1]\, e^{-(a+k)\,\Delta z_1} \right\} \tag{4.75}$$

and

$$\int_0^{\Delta z_1} e^{-k\,z} \mathrm{d}z = \frac{1}{k} \left\{ 1 - e^{-k\,\Delta z_1} \right\} \tag{4.76}$$

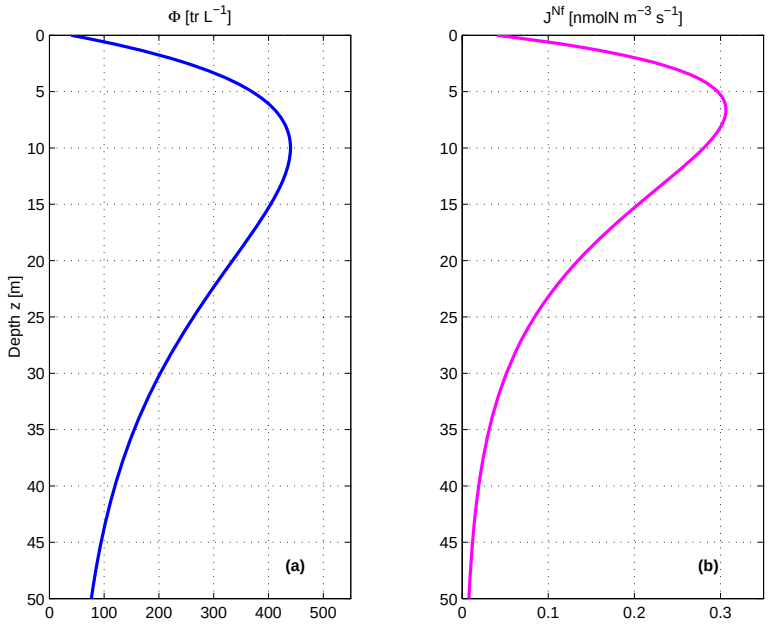

FIG. 4.11. Depth profiles within the top layer for (a) diazotroph concentration $\Phi(z)$ and (b) dinitrogen fixation source term J^{Nf}.

Denitrification is parameterized as a loss of NO_3 whose column integral is equal to input by DNF so that the global total pool of fixed N is constant. Below the top model layer, denitrification is proportional to the detrital remineralization rate

$$J_k^{Nf} = -F_{Nf} \times \frac{r_e\, D_k}{\sum_{k=2}^{n} r_e\, D_k} \tag{4.77}$$

where n is the number of model layers, so that denitrification occurs predominantly in the layers just below the surface layer (Codispoti *et al.* 2001) and then decreases exponentially with depth.

4.8 Iron limitation

In order to account for regions of apparent iron (Fe) limitation of phytoplankton growth despite availability of nutrients (Martin and Fitzwater 1988; Fung *et al.* 2000), a surface ocean mask of an iron-limiting factor L_{Fe} was devised.

It was derived, for every surface ocean grid cell, from normalized monthly observational estimates of the climatological annual minimum nitrate concentration NO_3^{min} at that location (Conkright *et al.* 2002). The resulting spatially varying map (Fig. 4.12, top panel) had higher nutrient concentrations in known regions of suspected Fe limitation of phytoplankton growth.

These values were then converted to values for the iron limitation factor L_{Fe}

$$L_{Fe} = 1.0 - \log_{10}\left(NO_3^{min} + 1\right) \tag{4.78}$$

assuming that the lowest concentration of NO_3 observed during the seasonal cycle is proportional to the degree of iron limitation, indicating likely limitation of growth by Fe in the Southern Ocean, the northwest North Pacific, and to a lesser extent in the eastern Equatorial Pacific. The global distribution of L_{Fe} is shown in (Fig. 4.12, bottom panel).

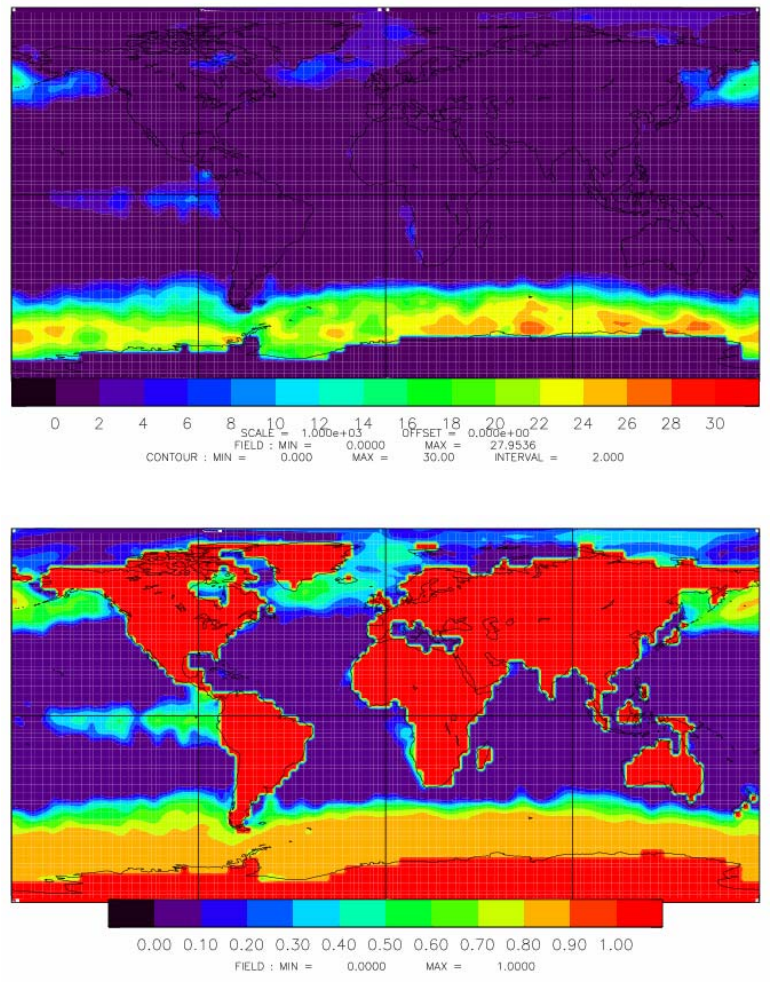

FIG. 4.12. Top: Map of monthly data estimates of the climatological yearly minimum NO_3 from World Ocean Atlas 2001; Bottom: Map of corresponding L_{Fe} limitation factors.

Chapter 5

Model initial conditions and forcing

The modified NPZD+Chl ecosystem model coupled with the inorganic carbon module was initialized from an equilibrium state of the physical model (T, S, u, v) after 4000 years of integration of the physical model. The N tracer was initialized from data estimates (Key *et al.* 2004; Conkright *et al.* 2002); P, Z, D and Chl were initialized with horizontally-uniform profiles, exponentially decreasing with depth to a small background value. In practice, because of their relatively high "turnover" rates, P, Z, D, and Chl "spin-up" within a few years. Dissolved inorganic carbon and total alkalinity were initialized with global mean uniform values as in the OCMIP II protocols.

For a spinup to a pre-industrial equilibrium, the model was forced with wind stress, heat and freshwater fluxes, solar irradiance, sea ice extent, and atmospheric pressure from a multi-century CGCM run. Sea surface temperature (SST) and salinity (SSS)

are additionally restored to observed monthly climatology on a one-month timescale and an annual climatology on six-month timescale, respectively. Atmospheric pCO_2 is kept at a constant value representative of pre-industrial levels (288 ppm). The model is considered to reach steady state when the global integral air-sea exchange of CO_2 is less than 0.01 PgC y^{-1}.

In coupled mode, the ocean carbon model is part of the coupled carbon GCM and is forced daily by the AGCM with a flux of carbon being exchanged daily between the oceanic and atmospheric component of the coupled carbon model.

Chapter 6

Summary

We have implemented an NPZD+Chl ecosystem model similar to the 1-D model by Denman and Peña (1999) in the CCCma global ocean carbon model. The five ecosystem variables are nitrogen, phytoplankton, zooplankton, detritus and chlorophyll. These are added, in a full carbon model simulation, to dissolved inorganic carbon and total alkalinity for a total of seven prognostic variables related to the ocean carbon cycle.

Phytoplankton growth is limited by light, temperature, nitrogen, and iron. Detritus sinks with a constant speed, and export production is calculated at the bottom of the euphotic zone. $CaCO_3$ formation is treated implicitly as a temperature-varying fraction of the export production which then decreases with depth due to $CaCO_3$ redissolution. The NPZD+Chl ecosystem is coupled to the inorganic/solubility pump via sources/sinks of DIC and TA from respective sources/sinks of $CaCO_3$ and the nutrient N.

Table 1: CMOC ecosystem module parameters and their typical values.

Parameter	**Symbol**	**Value**	**Units**
PAR fraction of irradiance	a_{par}	0.45	—
PAR attenuation coefficient for seawater	k_w	0.04	m^{-1}
PAR attenuation coefficient for chlorophyll	k_{Chl}	0.03	$m^{-1}\ (mg\,Chl\,m^{-3})^{-1}$
Initial slope of P-I curve	α_{Chl}	5.0	$mg\,C \cdot (mg\,Chl)^{-1} \cdot (W\,m^{-2})^{-1} \cdot d^{-1}$
Maximum Chl:C ratio	θ_m	0.03	$mg\,Chl \cdot (mg\,C)^{-1}$
Chl relaxation time scale	τ_θ	2.0	d
Activation energy for growth	E_P	33.26	$kJ\,mol^{-1}$
Activation energy for remineralization	E_D	45.73	$kJ\,mol^{-1}$
Reference maximum ocean temperature	$T_{ref}^{v_m}$	30.0	°C
Reference maximum photosynthesis rate at $T_{ref}^{v_m}$	v_m^{ref}	3.0	d^{-1}
Nitrogen half-saturation constant	K_N	0.1	$mmolN\,m^{-3}$
Phytoplankton mortality to detritus	m_{pd}	0.05	d^{-1}
Phytoplankton aggregation parameter	m_{aggr}	0.1	$d^{-1} \cdot (molN\,m^{-3})^{-1}$
Zooplankton maximum grazing rate	r_m	2.0	d^{-1}
Zooplankton grazing half-saturation constant	K_P	0.2	$mmolN\,m^{-3}$
Zooplankton assimilation efficiency	g_a	0.7	—
Zooplankton losses to nitrogen	m_{zn}	0.2	d^{-1}
Zooplankton losses to detritus	m_{zd}	0.05	d^{-1}
Zooplankton quadratic mortality	m_{zd_2}	0.1	$d^{-1} \cdot (molN\,m^{-3})^{-1}$
Detritus sinking speed	w_s	10.0	$m\,d^{-1}$
Reference maximum detritus remineralization rate	r_e^{ref}	0.15	d^{-1}
Maximum rain ratio	$R_{Ci:Co}^m$	0.085	—
Rain ratio half-point temperature	T_{Ci}^r	10.0	°C
Rain ratio scaling factor	a_{Ci}	0.6	K^{-1}
$CaCO_3$ redissolution depth scale	d_{Ci}	2700.0	m
Maximum reference diazotroph concentration	Φ_{ref}^{Nf}	500.0	$trichomes\,L^{-1}$
Surface reference diazotroph concentration	Φ_0	50.0	$trichomes\,L^{-1}$
Inverse depth of diazotroph concentration maximum	a_{Nf}	0.1	m^{-1}
Maximum reference rate of dinitrogen fixation	P_{ref}^{Nf}	3.0	$pmolN\,trichome^{-1}\,h^{-1}$
Maximum reference $Nfix$ surface irradiance	I_{max}^{Nf}	350.0	$W\,m^{-2}$
Maximum reference $Nfix$ sea-surface temperature	T_{max}^{Nf}	30.0	°C
Minimum reference $Nfix$ sea-surface temperature	T_{min}^{Nf}	20.0	°C
Redfield C:N ratio	$R_{C:N}$	6.6	$molC \cdot (molN)^{-1}$
Depth of euphotic zone	d_{eu}	100.0	m
Thickness of surface model layer	Δz_1	50.0	m

Acknowledgments. We are very grateful to various groups that have made their data products available through the Climate Data Library, and especially to all of the investigators involved in GLODAP. Reiner Schlitzer graciously provided his export fields to us, and Ed Laws made his algorithm available to the community via US-JGOFS. We are also grateful to Warren Lee and Bill Merryfield for their efforts in development and maintenance of the CCCMA ocean model and the system support staff in Victoria and Dorval. Debby Ianson and Bill Merryfield made helpful comments on an earlier draft of this paper. This research was supported in part by CFCAS network funds awarded to N. Roulet of McGill University and to KLD under the Canadian Global Coupled Carbon Climate Model (CGC^3M) network.

REFERENCES

Abramowitz, M., and I. Stegun, 1965: *Handbook of mathematical functions, with formulas, graphs, and mathematical tables,*, Dover Publications, New York, 1046pp pp.

Arrhenius, S., 1889: On the reaction velocity of the inversion of cane sugar by acids, *Zeitschrift für Physikalische Chemie*, **4**, 226, Reproduced in *Selected Readings in Chemical Kinetics. 1967* (edited by M.H.Back, and K.J. Laidler), Pergamon, Oxford.

Baker, K., and R. Frouin, 1987: Relation between photosynthetically available radiation and total insolation at the ocean surface under clear skies, *Limnol. Oceanogr.*, **32**, 1370–1377.

Behrenfeld, M., O. Prasil, M. Babin, and F. Bruyant, 2004: In search of a physiological basis for covariations in light-limited and light-saturated photosynthesis, *J. Phycol.*, **40**, 4–25.

Bissett, W., J. Walsh, D. Dieterle, and K. Carder, 1999: Carbon cycling in the upper waters of the Sargasso Sea: I. Numerical simulation of differential carbon and nitrogen fluxes, *Deep-Sea Res. I*, **46**, 205–269.

Capone, D., J. Zehr, H. Paerl, B. Bergman, and E. Carpenter, 1997: *Trichodesmium*, a globally significant marine cyanobacterium, *Science*, **276**, 1221–1229.

Christian, J., M. Verschell, R. Murtugudde, A. Busalacchi, and C. McClain, 2002: Biogeochemical modelling of the tropical Pacific Ocean. I: Seasonal and interannual variability, *Deep-Sea Res. II*, **49**, 509–543.

Codispoti, L., J. Brandes, J. Christensen, A. Devol, S. Naqvi, H. Paerl, and T. Yoshinari, 2001: The oceanic fixed nitrogen and nitrous oxide budgets: Moving targets as we enter the anthropocene?, *Scientia Marina*, **65**, 85–105.

Conkright, M., H. Garcia, T. O'Brien, R. Locarnini, T. Boyer, C. Stephens, and J. Antonov, 2002: World Ocean Atlas 2001, Volume 4: Nutrients, in *NOAA Atlas NESDIS 52*, vol. 4, edited by S. Levitus, p. 392pp, U.S. Government Printing Office, Wash., D.C.

Denman, K., and A. Peña, 1999: A coupled 1-D biological/physical model of the northeast

subarctic Pacific Ocean with iron limitation, *Deep-Sea Res. II*, **46**, 2877–2908.

Dickson, A., 1981: An exact definition of total alkalinity and a procedure for the estimation of alkalinity and total CO_2 from titration data, *Deep-Sea Res.*, **28**, 609–623.

Drange, H., 1994: An isopycnic coordinate carbon cycle model for the North Atlantic, and the possibility of disposing of fossil fuel CO_2 in the ocean, Ph.D. thesis, p. 286pp, Nansen Environm. Remote Sensing Centr. and Dep. of Math., Univ. of Bergen, Bergen, Norway.

Eppley, R., 1972: Temperature and phytoplankton growth, *Fish. Bull.*, **70**, 1063–1085.

Flato, G., G. Boer, W. Lee, N. McFarlane, D. Ramsden, M. Reader, and A. Weaver, 2000: The Canadian Centre for Climate Modelling and Analysis global coupled model and its climate, *Climate Dynamics*, **16**, 451–467.

Flynn, K., 2001: A mechanistic model for describing dynamic multi-nutrient, light, temperature interactions in phytoplankton, *J. Plankton Res.*, **23**, 977–997.

Fung, I., S. Meyn, I. Tegen, S. Doney, J. John, and J. Bishop, 2000: Iron supply and demand in the upper ocean, *Global Biogeochem. Cycles*, **14**, 281–296.

Geider, R., H. MacIntyre, and T. Kana, 1996: Dynamic model of photoadaptation in phytoplankton, *Limnol. Oceanogr.*, **41**, 1–15.

Geider, R., H. MacIntyre, and T. Kana, 1997: Dynamic model of phytoplankton growth and acclimation: responses of the balanced growth rate and the chlorophyll a:carbon ratio to light, nutrient limitation and temperature, *Mar. Ecol. Prog. Ser.*, **148**, 187–200.

Geider, R., H. MacIntyre, and T. Kana, 1998: A dynamic regulatory model of phytoplanktonic acclimation to light, nutrients, and temperature, *Limnol. Oceanogr.*, **43**, 679–694.

Gent, P., and J. McWilliams, 1990: Isopycnal mixing in ocean circulation models, *J. Phys. Oceanogr.*, **20**, 150–155.

Harris, G., 1980: The measurement of photosynthesis in natural populations of phytoplankton, in *The physiological ecology of phytoplankton*, edited by I. Morris, pp. 129–187, Blackwell, Oxford.

Iglesias-Rodriguez, M., C. Brown, S. Doney, J. Kleypas, D. Kolbere, Z. Kolber, P. Hayes, and P. Falkowski, 2002: Representing key phytoplankton functional grops in ocean arbon cycle models: Coccolithophorids, *Global Biogeochem. Cycles*, **16**, doi:10.1029/2001GB001454.

Kana, T., and P. Glibert, 1987: Effect of irradiances up to 2000 μE m^{-2} s^{-1} on marine *synechococcus* WH7803. 2. Photosynthetic responses and mechanisms, *Deep-Sea Res.*, **34**, 497–516.

Key, R., A. Kozyr, C. Sabine, K. Lee, R. Wanninkhof, J. Bullister, R. Feely, F. Millero, C. Mordy, and T.-H. Peng, 2004: A global ocean carbon climatology: Results from GLODAP, *Global Biogeochem. Cycles*, **18**, GB4031, doi:10.1029/2004GB002247.

Kirk, J., 1994: *Light and photosynthesis in aquatic ecosystems*, Cambridge University Press, Cambridge, 509pp pp.

Lefévre, N., A. Taylor, F. Gilbert, and R. Geider, 2003: Modelling carbon to nitrogen and carbon to chlorophyll *a* ratios in the ocean at low latitudes: Evaluation of the role of physiological plasticity, *Limnol. Oceanogr.*, **48**, 1796–1807.

Li, W., 1980: Temperature adaptation in phytoplankton: cellular and photosynthetic characteristics, in *Primary Productivity in the sea*, edited by P. Falkowski, pp. 259–279, Plenum Press, New York.

Li, W., and P. Dickie, 1987: Temperature characteristics of photosynthetic and heterotrophic activities: Seasonal variations in temperate microbial plankton, *Appl. Environ. Microbiol.*, **53**, 2282–2295.

Lima, I., and S. Doney, 2004: A three-dimensional, multinutrient, and size-structured ecosystem model for the North Atlantic, *Global Biogeochem. Cycles*, **18**, GB3019, doi: 10.1029/2003GB002146.

MacIntyre, H., T. Kana, T. Anning, and R. Geider, 2002: Photoacclimation of photosynthesis irradiance response curves and photosynthetic pigments in microalgae and cyanobacteria, *J. Phycol.*, **38**, 17–38.

Martin, J., and S. Fitzwater, 1988: Iron deficiency limits phytoplankton growth in the north-east Pacific subarctic, *Nature*, **331**, 341–343.

McCreary, J., K. Kohler, R. Hood, and D. Olson, 1996: A four-component ecosystem model of biological activity in the Arabian Sea, *Progress in Oceanogr.*, **37**, 193–240.

Millero, F., 1995: Thermodynamics of the carbon dioxide system in the oceans, *Geochim. Cosmochim. Acta*, **59**, 661–677.

Moore, J., S. Doney, J. Kleypas, D. Glover, and I. Fung, 2002: An intermediate complexity marine ecosystem model for the global domain, *Deep-Sea Res. II*, **49**, 403–462.

Morris, A., and J. Riley, 1966: The bromide/chlorinity and sulphate/chlorinity ratio in sea water, *Deep-Sea Res.*, **13**, 699–705.

Orcutt, K., F. Lipschultz, K. Gundersen, R. Arimoto, A. Michaels, A. Knap, and J. Gallon, 2001: A seasonal study of the significance of N_2 fixation by *trichodesmium* spp. at the Bermuda Atlantic Time-series Study (BATS) site, *Deep-Sea Res. II*, **48**, 1583–1608.

Platt, T., D. Bird, and S. Sathyendranath, 1991: Critical depth and marine primary production, *Proc. Royal Soc. London Ser.B*, **246**, 205–217.

Platt, T., C. Gallegos, and W. Harrison, 1980: Photoinhibition of photosynthesis in natural assemblages in marine phytoplankton, *J. Mar. Res.*, **38**, 687–701.

Platt, T., and S. Sathyendranath, 1993: Estimators of primary production for interpretation of remotely sensed data on ocean color, *J. Geophys. Res.*, **98**, 14,561–14,576.

Platt, T., S. Sathyendranath, and P. Ravindran, 1990: Primary production by phytoplankton: analytic solutions for daily rates per unit area of water surface, *Proc. Royal Soc. London Ser.B*, **241**, 101–111.

Raven, J., and R. Geider, 1987: Temperature and algal growth, *New Phytologist*, **110**, 441–461.

Riley, J., 1965: The occurence of anomalously high fluoride concentrations in the North Atlantic, *Deep-Sea Res.*, **12**, 219–220.

Rivkin, R., and L. Legendre, 2001: Biogenic carbon cycling in the upper ocean: Effects of

microbial respiration, *Science*, **291**, 2398–2400.

Spitz, Y., J. Moisan, and M. Abbott, 2001: Configuring an ecosystem model using data from the Bermuda Atlantic Time Series (BATS), *Deep-Sea Res. II*, **48**, 1733–1768.

Steele, J., and E. Henderson, 1992: The role of predation in plankton models, *J. Plankton Res.*, **14**, 157–172.

Uppström, L., 1974: Boron/chlorinity ratio of deep-sea water from the Pacific Ocean, *Deep-Sea Res.*, **21**, 161–162.

Wanninkhof, R., 1992: Relationship between wind speed and gas exchange over the ocean, *J. Geophys. Res.*, **97**, 7373–7382.

Weiss, R., 1974: Carbon dioxide in water and seawater: The solubility of a non-ideal gas, *Mar. Chem.*, **2**, 203–215.

Weiss, R., and B. Price, 1980: Nitrous oxide solubility in water and seawater, *Mar. Chem.*, **8**, 347–359.